Ion Mobility Spectrometry with Mass Spectrometry

6

Toshiki Sugai

6.1 Introduction

6.1.1 Mass Spectrometry and Ion Mobility Spectrometry

The advantages of mass spectrometry (MS) in terms of rich information, easy operation, and high throughput have been established since its invention, and they have been applied for many fields such as nanomaterials, biochemistry, and medical diagnostics. To expand the potential, the ion mobility spectrometry (IMS) combined with MS has been developed rapidly as a kind of hybrid measurement system, so called IMS/MS. IMS has close relationship with MS but also has unique properties for structural analyses and detection of intermolecular interaction [1, 2]. This IMS/MS has novel advantages originating from both systems which can be clarified by the discovery of C_{60} which resulted in Nobel Prize in chemistry in 1996 [3] and the following structural identifications of C_{60}. The detection method of C_{60} was MS with a laser vaporization cluster source developed by Nobel laureate R. Smalley. It would have been impossible without MS providing high sensitivity, high throughput, and high resolution for the discovery. However, the discovery also shows the limit of information obtained by MS: the final identification and structural determination were executed by NMR and X-ray diffraction, the so-called bulk measurement methods, with bulk production achieved by Krätchmer and Huffman in 1991 [4, 5, 6]. MS is powerful enough to identify "well-known materials" but is able to just show the "possibility of existence" for something new. IMS/MS, on the other hand, can tell not only the "soccer ball" structure of stable C_{60} fullerenes without help of other measurement methods but also some new structures of unstable C_{60} clusters [7, 8].

In this chapter, I will show the concept, the apparatus, and the potential of IMS/MS [9].

6.1.2 Concept of IMS and Difference Between MS and IMS

Figure 6.1 shows the concept of IMS. Both ions shown here consist of 60 carbon atoms but have different structures, so-called isomers. In IMS as well as in MS, ion movement under an electric field is observed. The differences are that IMS utilizes the steady movement dominated by the ion–gas

T. Sugai (✉)
Department of Chemistry, Toho University, 2-2-1 Minayama, Funabashi-shi,
Chiba 2748510, Japan
e-mail: sugai@chem.sci.toho-u.ac.jp

K. Hiraoka (ed.), *Fundamentals of Mass Spectrometry*, DOI 10.1007/978-1-4614-7233-9_6,

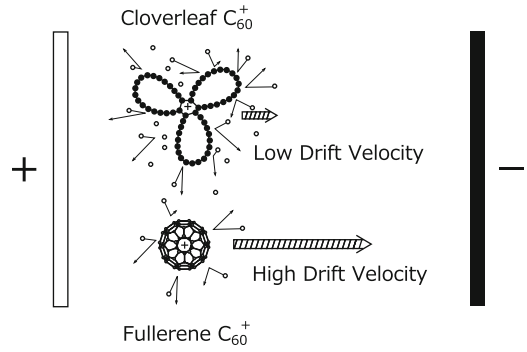

Fig. 6.1 Concept of ion mobility spectrometry. The mobility or the drift velocity of ions under electric fields reflects the structure of the ions and the interaction between the ions and the gas molecules. The *top figure* shows a cloverleaf structure of C_{60} with a small drift velocity and the *bottom figure* shows a fullerene structure with a large drift velocity. The *open circles* show the gas molecules interacting with the ion. The cloverleaf ion collides with the gas molecules more frequently or have more interaction than the fullerene ion, which results in the small mobility

interaction in a relatively high pressure gas, whereas MS utilizes the accelerated movement by the field in vacuum. The upper cloverleaf ion in the figure has more intense interaction or a larger collision cross section with the gas molecule and the lower fullerene one has less intense interaction or a smaller cross section. The consequence of those differences is the lower drift velocity of the cloverleaf isomer and the higher one of the fullerene. IMS can identify those isomers which MS cannot distinguish.

The difference between MS and IMS is shown in Fig. 6.2. Both IMS and MS are based on processes and interaction with the difference of several orders of the magnitude in energy and time. The high energy acceleration in vacuum of tens of eV to keV is utilized in MS where an ion must be stable without collision for around μs to be identified as a single species. When the ion has even single collision, the high energy collision induced dissociation (CID) is invoked and numbers of different ions are produced. It is usually difficult to investigate the weak interaction with thermal energy of several meV in MS.

On the other hand, the low energy thermal collisions in high pressure gas together with the movement by the field are utilized in IMS where very weak interaction can be observed through the drift velocity. Even if the complex between ion and gas is unstable with much shorter life time than μs, we can detect the complex and the interaction by the change of the drift velocity through many collisions. This sensitivity in terms of the weak interaction provides us the new tool to have fine information on ions like isotope effects and chiral effects suggesting the potential of IMS to explore novel scientific fields.

6.2 Kinetics in IMS

In IMS, ions obey kinetics under a static electric field as well as in MS [1, 10]. The ion movement in IMS is strongly affected by collisions with gas molecules, whereas it is dominated only by the field in MS without collision in vacuum where an ion with a mass of m and a charge of q is accelerated by the electric field of a vector $\overrightarrow{E}$ with the magnitude $E \equiv |\overrightarrow{E}|$. Throughout this chapter a physical quantity such as an electric field is represented by E or $\overrightarrow{E}$ where the latter one stresses the meaning of a vector. The velocity of the ion keeps increasing in MS with the acceleration of Eq / m. In IMS under the same

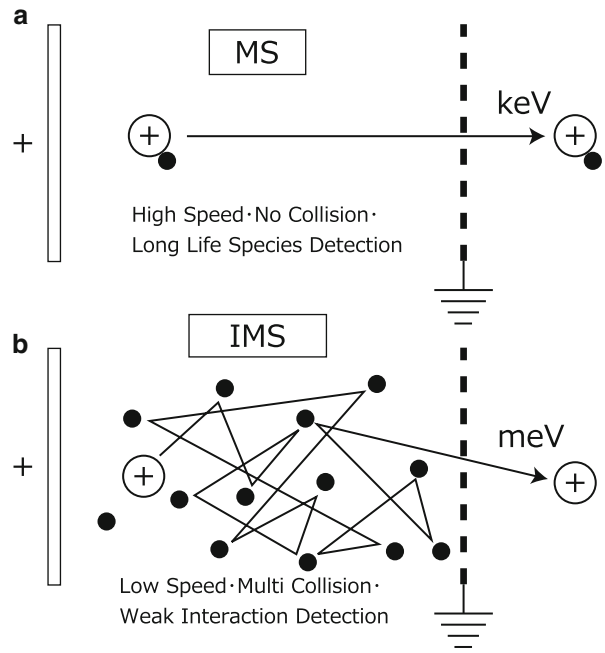

Fig. 6.2 The difference between (**a**) MS and (**b**) IMS. MS utilizes relatively high energy (tens of eV to keV) acceleration processes and the detected ion must be stable without collision during around μs in the acceleration. Even when the ion–molecule complex is unstable with short lifetime much less than μs because of the weak interaction, they can be detected with many ion–molecule collisions or many chance to form the complex in long-term observation

electric field of E, the velocity of the ion converges on a drift velocity of $v_d(E/N)$ as a function of the field of E and a molecular gas density of N. Since the obtained drift velocity reflects the interaction between the ion and the gas molecule which strongly depends on the ion structure, the structural information is deduced from the IMS measurement. This ion movement in IMS is categorized into two conditions: the low field condition and the high field condition [1, 10]. In the low field condition, it is dominated by the thermal collision with the perturbation of the field acceleration. In the latter case, on the other hand, the field acceleration is comparable to the collision, which will be discussed later.

6.2.1 Low Field Condition

The low field condition is realized by low E/N with the high pressure or the low field where the field effect is much lower than that of the collision. In this condition the velocity of the ion converges on the drift velocity which is proportional to the field E as described in Eq. (6.1).

$$v_d = KE. \tag{6.1}$$

This K is defined as an ion mobility. It has a close relationship with the structure of the ion so that we can deduce the structural information from the mobility.

Here the mobility is analyzed through the movement in gas under the static electric field. Figure 6.3 shows the collision processes of IMS, where the ion and the gas molecules are regarded as hard

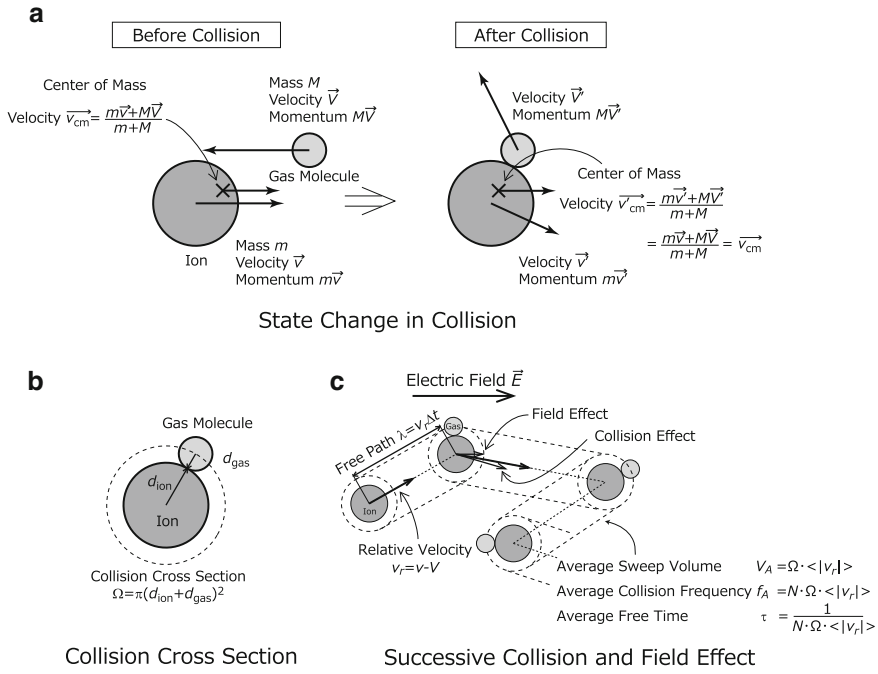

Fig. 6.3 (**a**) The states of an ion and a gas molecule before and after the collision. The velocities of the ion and the gas of $\vec{v}$ and $\vec{V}$ are changed to those of $\vec{v}'$ and $\vec{V}'$, respectively. The velocity of the center of mass $\overrightarrow{v_{cm}}$ is constant. (**b**) The collision cross section $\Omega = \pi\left(d_{ion} + d_{gas}\right)^2$ between the ion and the gas molecule. It determines the collision frequency between the ion and the gas. The collision occurs when the distance between the ion and the gas molecule is shorter than $d_{ion} + d_{gas}$. (**c**) Successive collision processes. The ion is accelerated by the field during the so-called free path where no collision occurs. After these collision processes, the ion drifts in the buffer gas. The relative velocity of v_r, the average sweep volume of V_A, the average collision frequency of f_A, and the mean free time τ are described in the text

spheres with the constant collision cross section and without internal freedom like vibrations and rotations. The total collision energy is distributed only into the kinetic energy of each particle. The collision cross section is independent of the field, the temperature of the gas, and the energy. Figure 6.3a shows the kinetic processes in the collision where the masses of the ion and the gas molecules are defined as m and M, respectively. The velocities of the ion and the gas change from $\vec{v}$ and $\vec{V}$ to $\vec{v}'$ and $\vec{V}'$, respectively, keeping the velocity of the center of mass $\overrightarrow{v_{cm}}$ constant. As described in Fig. 6.3b, the radii of the ion and the gas molecule are defined as d_{ion} and d_{gas}, respectively. The collision cross section (Ω) is described as $\Omega = \pi\left(d_{ion} + d_{gas}\right)^2$, which is independent of the temperature of the gas, the velocity, and the field. Whenever the distance between the ion and the gas molecule is less than $d_{ion} + d_{gas}$, they must collide with each other.

Figure 6.3c shows the successive collisions between the ion and the gas molecules under the field. The ion is accelerated by the field during free time Δt between the collisions where the ion moves without collision in the path of $\lambda = v_r \Delta t$, where v_r is the relative velocity defined as the difference between the velocities of the ion and the gas molecule like

$$\vec{v}_r \equiv \vec{v} - \vec{V}. \tag{6.2}$$

After these collision processes, the ion drifts in the buffer gas in macroscale and this movement is detected in IMS observation. The field effect becomes more significant with the longer Δt. The average Δt defined as τ determines the drift velocity in whole processes which is calculated as the inverse of the average collision frequency $1/f_{\mathrm{A}}$. Here f_{A} is the average number of collisions between the ion and the gas molecules in unit time. As shown in Fig. 6.3c, f_{A} is deduced from the number of the gas molecules in sweep volume V_{A} which is defined as $\Omega \cdot \langle |\overrightarrow{v_{\mathrm{r}}}| \rangle$. When the ion is assumed to move in frozen gas molecules, we have the frequency as $f_{\mathrm{A}} = N \cdot \Omega \cdot \langle |\overrightarrow{v_{\mathrm{r}}}| \rangle$, where N is the molecular gas density. Finally the average free time of τ is represented as [1, 10, 11]

$$\tau = 1/f_{\mathrm{A}} = \frac{1}{N\langle |\overrightarrow{v_{\mathrm{r}}}| \rangle \Omega}. \tag{6.3}$$

The ion has the constant drift velocity in IMS observation, the acceleration or the momentum gain by the field is lost in average by the collisions. The gain is calculated with the impulse of

$$m\left\langle \overrightarrow{v} - \overrightarrow{v'} \right\rangle = \overrightarrow{F} \times \tau = q\overrightarrow{E}\tau, \tag{6.4}$$

where $\overrightarrow{F}$ is the field force applied to the ion. This momentum gain is converted into acceleration of the colliding gas molecule, which is represented as

$$M\left\langle \overrightarrow{V'} - \overrightarrow{V} \right\rangle = M\left\langle \overrightarrow{V'} \right\rangle - M\left\langle \overrightarrow{V} \right\rangle = q\overrightarrow{E}\tau, \tag{6.5}$$

where $\langle\rangle$ represents the average of the whole processes. Here the gas molecules do not move macroscopically, which is equivalent to the zero average velocity of the gas molecules before the collision represented as

$$\langle \overrightarrow{V} \rangle = 0. \tag{6.6}$$

From Eqs. (6.5) and (6.6) we have

$$\left\langle \overrightarrow{V'} \right\rangle = \frac{q\overrightarrow{E}\tau}{M}. \tag{6.7}$$

Through the collision processes, v_{r} randomly varies by the slight changes in positions and angles because of actual complicated structures of the ion and the gas molecule. The consequence is that the average v_{r} on the whole molecules is reduced to zero, which is represented as

$$\left\langle \overrightarrow{v'_{\mathrm{r}}} \right\rangle \equiv \langle \overrightarrow{v'} - \overrightarrow{V'} \rangle = 0 \Leftrightarrow \left\langle \overrightarrow{v'} \right\rangle = \left\langle \overrightarrow{V'} \right\rangle. \tag{6.8}$$

The momentum conservation in the collision process tells us the following relation with $\langle \overrightarrow{v} \rangle, \langle \overrightarrow{v'} \rangle$ as

$$m\langle \overrightarrow{v} \rangle + M\left\langle \overrightarrow{V} \right\rangle = m\left\langle \overrightarrow{v'} \right\rangle + M\left\langle \overrightarrow{V'} \right\rangle. \tag{6.9}$$

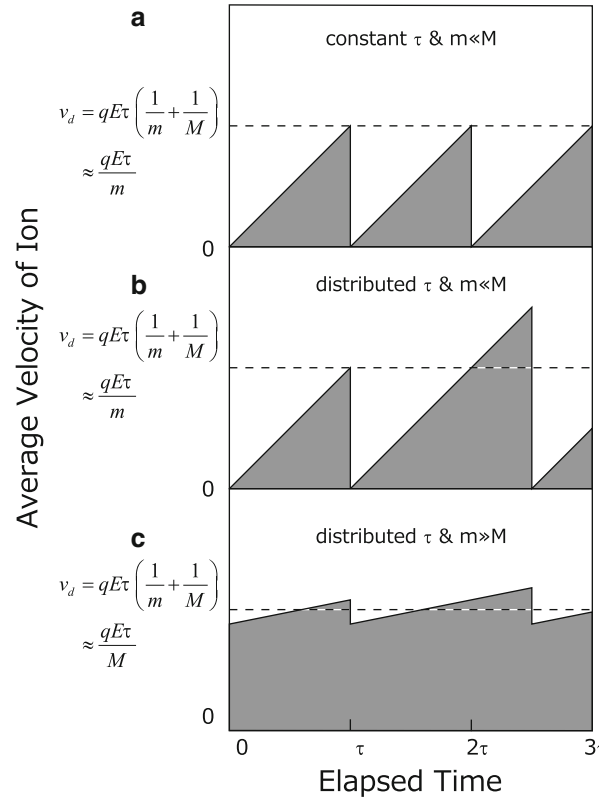

Fig. 6.4 The time profile of the average velocity of an ion in IMS. The unit of horizontal line is the average free time τ. The ion is accelerated by the field in the free time and is decelerated by the collision. (**a**) The profile when the mass of ion is much smaller than that of the gas molecule with periodic collisions, (**b**) in the same mass condition as (**a**) with irregular collisions represented as Poisson distribution, and (**c**) in the condition that the mass of ion is much larger than that of the gas molecule with irregular collisions

With Eqs. (6.6)–(6.9), the average ion velocity just before the collision, which is the same as the drift velocity of v_d [1, 10], is turned out to be

$$v_d \equiv \left|\langle \overrightarrow{v} \rangle\right| = qE\tau\left(\frac{1}{m}+\frac{1}{M}\right). \tag{6.10}$$

Equation (6.10) is interpreted as follows. When the mass of ion is much smaller than that of the gas molecule, $m \ll M$, Eq. (6.10) is reduced to $v_d = qE\tau/m$ with $1/m \gg 1/M$. This case corresponds to the situation that the gas is heavy enough to stand still and the ion is reflected to random direction in the collision processes. This process results in zero average velocity of the ion after the collision which is followed by the field acceleration to $\langle \overrightarrow{v'} \rangle = qE\tau/m$ until the next collision. The lighter the ion is, the higher the drift velocity we have with the larger acceleration effect.

This time dependence of the average ion velocity is shown in Fig. 6.4a, b. When the collision occurs every τ (Fig. 6.4a) the average ion velocity is represented as a periodic sawtooth wave with the average velocity of $v_d = qE\tau/(2m)$. Actually the collision does not take place periodically but randomly where the free time varies with Poisson distribution of $p(t) = \frac{1}{\tau}\exp(-t/\tau)$. Here $p(t)$ is the probability function. In this situation, the average ion velocity is represented as an irregular sawtooth wave (Fig. 6.4b) so that the time average is obtained as $v_d = qE\tau/m$ since the average of the free time between the successive collisions is 2τ [11].

When the mass of the ion is much larger than that of the gas molecule, $m \gg M$, on the other hand, Eq. (6.10) is reduced to $v_d = qE\tau/M$, where almost no velocity change occurs through the collision and the field acceleration. The profile of the velocity is shown in Fig. 6.4c where we have

$$v = v'. \tag{6.11}$$

The momentum gain of the ion by the field is transferred to the gas molecule by the collision where the average velocity of the gas molecule is changed from zero in Eq. (6.6) to

$$\langle \overrightarrow{V'} \rangle = qE\tau/M. \tag{6.12}$$

Equations (6.8), (6.11), and (6.12) show that this average velocity of the gas molecule after the collision is the same as that of the ion represented as

$$\langle \overrightarrow{v} \rangle = \langle \overrightarrow{v'} \rangle = v_d = \langle \overrightarrow{V'} \rangle = qE\tau/M. \tag{6.13}$$

The smaller the mass of the gas molecule is, the higher drift velocity we have with the lower loss of the field acceleration.

For the analysis of actual IMS measurement, v_d should be obtained as a function of a gas temperature T together with the molecular gas density N and the collision cross section Ω. When the free time τ in Eq. (6.3) is introduced to Eq. (6.10), the drift velocity is represented as

$$v_d = \frac{qE}{N\langle |\overrightarrow{v_r}| \rangle \Omega} \left(\frac{1}{m} + \frac{1}{M} \right). \tag{6.14}$$

To introduce the gas temperature T the average velocity of $\langle |\overrightarrow{v_r}| \rangle$ is approximated with root mean approximation as

$$\langle |\overrightarrow{v_r}| \rangle \approx \sqrt{\langle v_r^2 \rangle} = \sqrt{\left\langle \left(\overrightarrow{v} - \overrightarrow{V} \right)^2 \right\rangle} = \sqrt{v^2 - 2\left\langle \overrightarrow{v} \cdot \overrightarrow{V} \right\rangle + V^2} = \sqrt{\frac{3k_B T}{m} + \frac{3k_B T}{M}}, \tag{6.15}$$

where $\left\langle \overrightarrow{v} \cdot \overrightarrow{V} \right\rangle$ is reduced to zero because of the independence of v and V with Eq. (6.6) [1, 10, 11]. With introduction of Eqs. (6.15) and (6.14), the drift velocity is summarized as

$$v_d = \frac{1}{\sqrt{3}} \frac{qE}{N} \left(\frac{1}{m} + \frac{1}{M} \right)^{1/2} \left(\frac{1}{k_B T} \right)^{1/2} \frac{1}{\Omega}. \tag{6.16}$$

The N and T dependence comes from the fact that τ is inverse of the collision frequency which is proportional to N and $\sqrt{T}$, respectively. The dependence on m and M, on the other hand, comes from two effects: the momentum effect in Eq. (6.10) and the thermal velocity effect in Eq. (6.2). The momentum transfer and the thermal velocity effects are proportional to $\left(\frac{1}{m} + \frac{1}{M}\right)$ and $\left(\frac{1}{m} + \frac{1}{M}\right)^{-1/2}$, respectively, so that we have the mass dependence of $\left(\frac{1}{m} + \frac{1}{M}\right)^{1/2}$ in Eq. (6.16). The approximation used in Eq. (6.16) is corrected with a more precise treatment as [1, 10, 11]

$$v_{\mathrm{d}} = \frac{3}{16}\frac{qE}{N}\left(\frac{1}{m}+\frac{1}{M}\right)^{1/2}\left(\frac{2\pi}{k_{\mathrm{B}}T}\right)^{1/2}\frac{1}{\Omega}. \tag{6.17}$$

With Eqs. (6.1) and (6.17), the mobility K is represented as

$$K = v_{\mathrm{d}}/E = \frac{3}{16}\frac{q}{N}\left(\frac{1}{m}+\frac{1}{M}\right)^{1/2}\left(\frac{2\pi}{k_{\mathrm{B}}T}\right)^{1/2}\frac{1}{\Omega}, \tag{6.18}$$

Thus the mobility K observed in IMS contains the information on the structure of ions which is elucidated from the cross section Ω in Eq. (6.18).

Typical ambient pressure IMS/MS measurement [12] is performed at 300 K in 500 Torr He. The estimated cross section from the observed mobility with the analysis of Eq. (6.18) is $1.\ 34 \times 10^{-14}\mathrm{cm}^2$. The hard sphere model tells that the cross section of C_{60} in He is $\Omega = 1.37 \times 10^{-14}\,\mathrm{cm}^2$ with $r_{C_{60}} = 3.5$ Å obtained by X-ray diffraction [6] together with the van der Waals radii of helium and carbon atoms of $r_{\mathrm{He}} = 1.\ 4$ Å and $r_{\mathrm{C}} = 1.\ 7$ Å. This good agreement shows that the hard sphere model describes the essence of IMS.

6.2.2 High Field Condition

The discussion so far is based on the low field model where the field acceleration is much smaller than the collision effect. Here the high field model is described in which the field effect is comparable to the collision effect [1, 10]. In this condition, the collision frequency and its effect increase as the field increases, whereas they are independent of the field in the low field condition. The field acceleration is analyzed by the collision energy distribution [1, 10], which is represented as

$$\begin{aligned}\frac{1}{2}m\left\langle v^2 - v'^2\right\rangle &= \frac{1}{2}M\left\langle V'^2 - V^2\right\rangle \\ &= qEv_{\mathrm{d}}\tau = \left(\frac{1}{m}+\frac{1}{M}\right)^{-1}v_{\mathrm{d}}^2.\end{aligned} \tag{6.19}$$

Here the first row of Eq. (6.19) shows that the energy loss of the ion is equal to the energy gain of the gas molecule in the collision since there is no internal freedom like rotations or vibrations. The second row represents the energy gain of the ion by the field acceleration with the relationship between τ and v_{d} in Eq. (6.10). Equation (6.19) is further represented with the relative velocity of v_{r} and the velocity of the center of mass of v_{cm}. The ion velocities before and after the collision v and v' are represented as [1, 10, 11]

$$\overrightarrow{v} = \overrightarrow{v_{\mathrm{cm}}} + \frac{M}{m+M}\overrightarrow{v_{\mathrm{r}}}, \tag{6.20}$$

$$\overrightarrow{v'} = \overrightarrow{v_{\mathrm{cm}}} + \frac{M}{m+M}\overrightarrow{v'_r}, \tag{6.21}$$

where we use the conservation of the velocity of the center of mass.

The energy loss of the ion is represented with those velocities as

$$\begin{aligned}\frac{m}{2}\left\{\langle v^2\rangle - \langle v'^2\rangle\right\} &= m\left\{\left\langle\left(\overrightarrow{v_{\mathrm{cm}}} + \frac{M}{m+M}\overrightarrow{v_{\mathrm{r}}}\right)^2\right\rangle - \left\langle\left(\overrightarrow{v_{\mathrm{cm}}} + \frac{M}{m+M}\overrightarrow{v_r'}\right)^2\right\rangle\right\} \\ &= 2\cdot\frac{m}{2}\left\langle\overrightarrow{v_{\mathrm{cm}}}\cdot\frac{M}{m+M}\overrightarrow{v_{\mathrm{r}}}\right\rangle \\ &= \frac{mM}{(m+M)^2}\langle mv^2 - MV^2\rangle, \end{aligned} \tag{6.22}$$

where we used the randomized relative velocity after the collision ($\langle v_{\mathrm{r}}'\rangle = 0$) in Eq. (6.8), the conservation of the absolute value of the relative velocity ($|v_{\mathrm{r}}| = |v_{\mathrm{r}}'|$) in an elastic collision, and the average of the square of the relative velocity ($\langle v_{\mathrm{r}}^2\rangle = \langle v^2\rangle + \langle V^2\rangle$). Finally this equation combined with Eq. (6.19) leads to the following energy relations of

$$\begin{aligned}\frac{m}{2}\left\{\langle v^2\rangle - \langle v'^2\rangle\right\} &= \frac{mM}{(m+M)^2}\left(\langle mv^2\rangle - \langle MV^2\rangle\right) = \frac{mM}{m+M}v_{\mathrm{d}}^2 \\ &\therefore \langle mv^2\rangle - \langle MV^2\rangle = (m+M)v_{\mathrm{d}}^2 \end{aligned} \tag{6.23}$$

and

$$\frac{1}{2}m\langle v^2\rangle = \frac{1}{2}M\langle V^2\rangle + \frac{1}{2}mv_{\mathrm{d}}^2 + \frac{1}{2}Mv_{\mathrm{d}}^2. \tag{6.24}$$

Equation (6.24) shows that the kinetic energy of the ion is the sum of the thermal energy, the kinetic energy of drift velocity, and the field acceleration energy distributed in the gas molecules [1, 10].

This high field effect results in higher v_{r} than that in the low field condition shown as

$$\begin{aligned}\langle v_{\mathrm{r}}^2\rangle = \langle v^2\rangle + \langle V^2\rangle &= \frac{3k_{\mathrm{B}}T}{m} + v_{\mathrm{d}}^2 + \frac{M}{m}v_{\mathrm{d}}^2 + \frac{3k_{\mathrm{B}}T}{M} \\ &= \left(\frac{1}{m}+\frac{1}{M}\right)3k_{\mathrm{B}}T + \left(1+\frac{M}{m}\right)v_{\mathrm{d}}^2 \\ &= \left(\frac{1}{m}+\frac{1}{M}\right)\left(3k_{\mathrm{B}}T + Mv_{\mathrm{d}}^2\right), \end{aligned} \tag{6.25}$$

where $\langle V^2\rangle = 3k_{\mathrm{B}}T/M$ is held even in the high field condition. This increase of the relative velocity in Eq. (6.25) is represented by the newly introduced effective temperature of T_{eff} defined as

$$T_{\mathrm{eff}} \equiv T + \frac{Mv_{\mathrm{d}}^2}{3k_{\mathrm{B}}} > T. \tag{6.26}$$

The effective temperature T_{eff} is higher than the gas temperature T. The drift velocity v_{d} is represented with T_{eff} as

$$\begin{aligned}v_{\mathrm{d}} &= \frac{qE}{N}\left(\frac{1}{m}+\frac{1}{M}\right)^{1/2}\left(\frac{1}{3k_{\mathrm{B}}T + Mv_{\mathrm{d}}^2}\right)^{1/2}\frac{1}{\Omega} \\ &= \frac{qE}{N}\left(\frac{1}{m}+\frac{1}{M}\right)^{1/2}\left(\frac{1}{3k_{\mathrm{B}}T_{\mathrm{eff}}}\right)^{1/2}\frac{1}{\Omega}, \end{aligned} \tag{6.27}$$

where the drift velocity is reduced with T_{eff} higher than T.

The high and the low field conditions are classified according to the index of T_{eff} with E/N as an ion acceleration parameter. The threshold for the low field is defined as the condition of $T_{\mathrm{eff}} \approx T$, which is equivalent to

$$\frac{E}{N} \ll \frac{3k_{\mathrm{B}}T\Omega}{q}\left(\frac{m}{m+M}\right)^{1/2}. \tag{6.28}$$

Thus E/N is an important index for IMS represented by a unit of Td (1 Td $\equiv 10^{-17}$ V cm^2). The low field condition is realized when E/N is around 1 Td while the high field of $E/N > 100$ Td is utilized in high field IMS [1, 2, 13, 14, 15].

The high E/N is not just for high T_{eff}. We can identify and manipulate molecular ions by applying high E/N. Those sophisticated measurements are enabled by controlling the internal freedom and the molecular interaction with E/N [1, 2, 15]. Although the kinetics of IMS discussed so far is based on hard sphere model without the internal freedom and the interaction, those freedom and interaction play significant roles in the actual measurement [1, 2, 10]. The collision energy is distributed in the rotations and the vibrations, which affects the momentum transfer in the collision and mobility eventually. The cross section also strongly depends on the temperature and the field because those parameters affect the interaction. With the effects the observed mobility show complicated behaviors on E/N from which we can deduce fine information on the internal freedom and the interaction of the ion [13, 14, 16,].

For example, the significant reduction of the mobility of diatomic molecular ions is observed at liquid He temperature, which is originated in enhancement of the momentum transfer from the ion to the gas molecules caused by excitation of a rotational mode [17]. Single atomic ion does not show these behaviors. The degree of the ion–molecule interaction is controlled by the relative velocity or the temperature in IMS [1, 18]. Both these parameters are widely investigated independently by changing T and T_{eff}. The observed phenomena are well understood as the effect of T_{eff} in wide scanning region of E, N, and T, even though T_{eff} and T should be strictly distinguished from each other. The collision processes observed in IMS is well represented as a two-body problem dominated by very local relationship between the accelerated ion and the colliding gas molecule [1].

6.3 Combination of IMS and Mass Spectrometry

6.3.1 Introduction

IMS can reveal the structural information which is hard to be deduced by MS. However the highest resolution of IMS is about 100 usually [12] or 1,000 when special combined methods are applied [19, 20]. This is much lower than that of MS up to 10^5–10^6. In terms of the sensitivity and the throughput, MS with electron multipliers also has much higher ones than those of IMS with a charge collection and an electronic amplifier. To have both advantages, IMS and MS are combined into a hybrid measurement system of IMS/MS recently [2, 9]. This novel hybrid measurement system is applied to wide research areas and is creating new scientific fields. Technically ion loss in the connection between IMS and MS is a serious problem so that effective ion transfer is the key technology. Two types of IMS/MS have been widely used: differential pumping system and ion injection system.

6.3.2 Ion Injection System

The ion injection system has been widely available since late 1980s revealing the cluster structures [21]. The system, at first, is developed to study the cluster reactions and the dissociation induced by the collision with buffer gas in the cell. By increasing up the cell pressure, IMS measurement is realized. The system is quite analogous to a mass spectrometer with CID, so-called MS/CID/MS. The IMS cell is located between the mass spectrometers of the magnetic sector or the quadrupole. Ions selected by the first mass spectrometer are injected into the cell with the pressure of several Torr and their mobility is analyzed by the cell and the second mass spectrometer. The second mass spectrometer is utilized as the arrival time measurement and the product analysis when dissociation or reaction occurs in the cell. The similarity to MS/CID/MS makes it easier to introduce IMS into existing mass spectrometers. Many commercial systems of this type have been developed recently.

The system has several advantages in addition to the similarity to MS/CID/MS: the utilization of the injection process for the structural control of the ion. The ion is heated through the injection with the energy up to several 100 eV against the flow from the IMS cell where the kinetic energy is converted to the internal energy of the ion. After entering inside the cell, the heated ion is immediately cooled down by the gas in the cell. The heat up and the cool down induce the structural conversion [8, 22], which are utilized for exploring new structures or investigating thermal stabilities of nascent structures. Disadvantage arising from this system is low resolution. Since the gas flow from the cell to MS is hazardous for the vacuum of MS and the flow prevents the ions to enter the cell, it is difficult to increase the gas pressure of the cell which usually results in the low resolution. To have much higher resolution with high pressure cell, ambient IMS/MS with differential pumping systems have been developed.

6.3.3 Differential Pumping System

In IMS/MS system, ions are lost during the transport between IMS and MS because of the pressure difference. To improve the efficiency, differential pumping IMS/MS system shown in Fig. 6.5 has been developed. The system itself has long history from 1960s [23]. However this system is widely available recently because of the experimental difficulties to detect diluted ions in the IMS cell. The system in Fig. 6.5 is developed by Prof. Jarrold and co-workers which consists of a laser desorption/ionization system, a high-pressure drift cell with a differential pumping system, and a quadrupole mass filter (QMS) with an ion detection system [24]. Ions like carbon clusters are produced by the laser system and are separated according to their mobility in the drift cell. They are finally mass analyzed by QMS to have two-dimensional IMS/MS profiles. The system can also be equipped with ESI for biomolecules.

In this system, an ion bunch is introduced in the cell with the static electric field and the mobility is observed by measuring the drift time as the time difference between the start of the drift or the ion injection and its end or the ion detection. The ion bunch is created by the ion shutter from a continuous ion source like ESI or the pulsed ion source of the laser system shown in the figure. This system is analogous to the time of flight mass spectrometer. The higher mobility ion has, the shorter drift time is observed. The correlation between the detected ion intensity and the drift time is observed as an IMS spectrum (drift profile).

Two distinct characteristics are realized in this system. One is the long drift cell with ambient buffer gas and high voltage of 10 kV with the low field condition to observe cross section. The other is the small aperture of ϕ 0.1 mm and the large-scale differential pumping system with diffusion

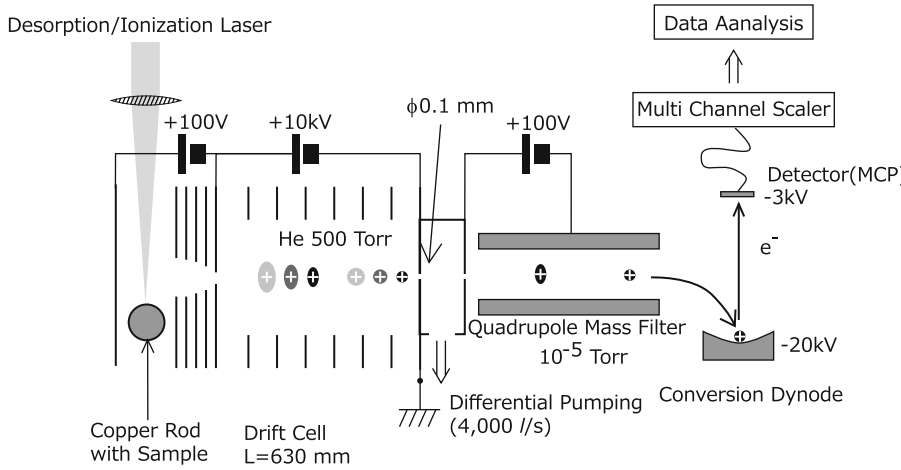

Fig. 6.5 A schematic diagram of a differential pumping high-resolution IMS/MS system. Produced ions are introduced to an IMS drift cell filled with high pressure buffer gas and they are separated according to their mobility. The ions then are passed through the differential pumping part and are introduced into a high vacuum quadrupole mass measurement system with detection and analysis functions

pumps (4,000 l/s). The ions are spatially separated in IMS and then are mass analyzed by QMS in vacuum under 10^{-5} Torr. Those kinds of differential pumping are often used in conventional MS system with an ambient ionization source like ESI. However the conventional MS system handles ions of the order of nA or 10^{10} ions/s which are directly introduced to the acceleration region of MS. The ions in this IMS/MS system, on the other hand, are spatially separated or diluted in the cell and then are transferred into MS. The experimental difficulties for the effective detection of such diluted ions are severer than the conventional MS with the ambient ion source.

The system shows still one of the highest IMS resolutions to observe the cross section. The resolution of this system is determined by the space resolution of the ion bunch [1, 9, 10]. When the ion bunch diffuses from the initial shape of a delta function to a Gaussian function, the resolution is proportional to $\sqrt{V/T}$ where V and T represent the whole voltage across the IMS cell and the gas temperature, respectively. This relation is due to the fact that the space separation increases when the drift effect exceeds the thermal diffusion. Here the thermal diffusion and the mobility compensate each other so that the drift length of the system does not affect the resolution apparently [1, 9, 10]. Many experimental results show that the resolution does not depend on the pressure and gas species indicating the universality of the resolution formula [13, 14, 25].

The higher voltage and the higher pressure with low E/N are crucial for high-resolution cross section measurements. Those measurements are realized with the cost of the detection efficiency, the system size, and complexity. Newly developed high-resolution IMS systems utilize much effective ion focusing systems with radio frequency AC high voltages (RF) [20, 26, 27]. The detection efficiency is also lowered by the low repetition frequency due to the long drift time. This problem has been solved in TOFMS by the so-called orthogonal acceleration keeping the high repetition rate to detect ions from continuous sources utilizing the fact that the ion velocities in TOFMS are much higher than those in the ion source. This method cannot be applied to this type IMS unfortunately since the drift velocity is comparable to the thermal velocity in the ion source.

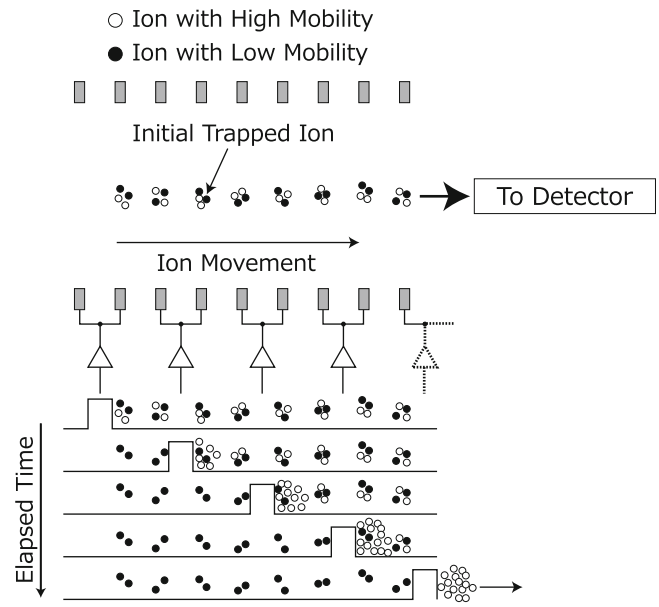

Fig. 6.6 A schematic diagram of a traveling wave (TW) ion mobility measurement system. Stacked ring electrodes with high-frequency (∼MHz) AC voltages accumulate ions at the center of each electrode. TW signals extract the ions with higher mobility (*open circles*) from those with lower mobility (*solid circles*) and eject them out of the system selectively for mass analyses

6.3.4 Traveling Wave System

IMS has serious problem in ion detection efficiency as described in Sect. 6.3.3 where the differential pumping system and the RF ion focusing system play significant roles. Here a new approach for handling the problem is shown: traveling wave ion mobility spectrometry (TWIMS) system developed by Waters Co. Ltd. [28]. Figure 6.6 shows the schematic diagram of the system. The system is equipped with a stacked ring ion guide (SRIG) where RF (∼MHz and ∼kV) is applied to co-axial ring electrodes to trap ions. Each adjacent electrode of SRIG has opposite polarity of RF so that intense and high-frequency electric fields are applied between the nearest electrodes. The frequency is so high that the ions cannot follow the polarity change of RF moving gradually from the inner rim to the center of SRIG according to the field strength, where the highest alternative field is applied at the rim and the lowest at the center. The ions then are trapped at the center of the each electrode since the trap potential is cylindrically symmetric with sinusoidal distortion along the center axis [28]. The potential is similar to that of linear ion trap (LIT) utilized for MS frequently but is different in the distortion along the axis. The trapped ion can be easily transported by applying bias voltages along the axis in SRIG while extra electrodes and complicated procedures are required in LIT to move the ions axially [29].

This distorted potential is crucial for TWIMS where the whole ions are utilized for the mobility measurements in contrast to the differential pumping system in Sect. 6.3.3. In the differential pumping system, the ions must be sliced as a thin bunch to have high resolution with the cost of losing intensity [28]. The procedure of TWIMS is shown in Fig. 6.6, where a waveform called traveling wave (TW) is applied to the SRIG electrodes for ion mobility with the superimposed RF for ion trap. TW is continuous moving waves with the field of tens of V/cm and the speed of hundreds of m/s, which drives the trapped ions out of SRIG to be detected by MS. The ions with higher mobility represented by open circles in the figure are effectively transferred to MS whereas those with smaller ones represented by filled circles are left in SRIG. Thus the mobility is measured by the eject

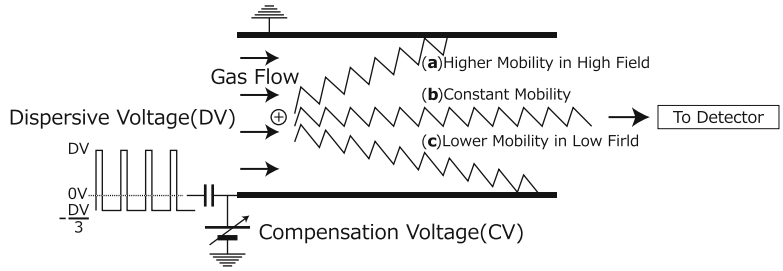

Fig. 6.7 A schematic diagram of a field asymmetric waveform ion mobility spectrometry (FAIMS) system. The system consists of two plates or coaxial cylinders between which ions are transferred to a detector or a mass spectrometer with flowing gas. Asymmetric high-frequency and high-voltage dispersion voltage (DV) and compensation voltage (CV) are applied to the electrodes. DV is asymmetric and its time average is zero. DV consists of a high positive voltage with a short period and a low negative voltage with a long period. When the ion has constant mobility, which is independent of the field, the ion can pass through the system as represented in (**b**) with $CV = 0$ condition. When the ion mobility increases or decreases with the increase of the field the ion movement is represented as (**a**) or (**c**) which cannot be detected. Those (**a**) and (**c**) type ions are detected by applying $CV < 0$ or $CV > 0$ for movement compensation, respectively

efficiency in TWIMS. High sensitivity with reasonable resolution is realized by tuning the voltage and the speed of TW. TWIMS is integrated as an ion injection system to observe the mobilities of mass selected ions. Since the injection system has the serious gas flow problem from IMS to MS, the cell pressure is limited to below several Torr and higher resolution is difficult to be achieved eventually [30]. TWIMS is the sensitivity-oriented measurement system.

TWIMS has achieved high sensitivity with SRIG by applying not only the DC bias but also the well-designed RF and TW waveforms. Those waveforms drive the ions with complicated trajectories and the high fields of the waveforms heat up and distort the ions [28, 31]. These effects make it difficult to convert the observed eject efficiencies or the time profile of TWIMS to the actual mobilities. For example, the linear relationship between the mobilities obtained from the TWIMS profile and the mobilities obtained by other measurement systems is fairly good for rigid and spherical molecules, whereas they are not held for asymmetric or soft molecules [32].

6.3.5 Field Asymmetric Waveform Ion Mobility Spectrometry

As described in Sect. 6.2, the low field should be applied to observe the cross section and the ion structure in IMS. In high field IMS, on the other hand, the mobility depends on the field because of the changes in the structures and the interaction leading to weak correlation between the observed mobility and the ion structure. This field dependence of mobility is sophisticatedly utilized in a field asymmetric waveform ion mobility spectrometry (FAIMS) to separate and distinguish ions [2, 15, 33].

Figure 6.7 shows the schematic diagram of FAIMS, where the system consists of two electrodes of plates or coaxial cylinders with gas flow. The observed ions transferred to a detector or a mass spectrometer by the gas flow under the fields of an asymmetric high frequency and high voltage waveform for dispersion (DV) and a static low voltage between the electrodes for compensation (CV). DV is asymmetric and its time average is zero. DV consists of a high positive voltage with a short period and a low negative voltage with a long period. The ion movement is classified in three types of (a)–(c). When the ion has a constant mobility, the ion can pass through the system as

represented in (b) with the condition of CV = 0. When the ion mobility increases or decreases as the field increases the ion movement are represented as (a) or (c). They collide with the electrodes and cannot be detected. Those (a) and (c) type ions are detected by applying CV < 0 or CV > 0 to compensate their movement to pass through the system like (b) condition. We can identify or separate ions of interest by tuning CV with steady DV and whole ion profiles are obtained as an intensity-CV correlation. Practically DV of several kV with frequency from several hundreds of kHz to MHz and CV of tens of V are applied to the electrodes with the gap from tens of μm to mm [15, 34].

FAIMS provides us the information not on the cross section but on the mobility dependence on the field which is difficult to interpret and is independent of most of the properties such as mass and size. This property is quite opposite to that of the cross section obtained by the low field IMS. The ion with larger cross section mostly have larger mass and size. The cross section is dependent on the mass and size, in other word, is not "orthogonal" to them. Here orthogonality means that two values are perpendicular, nonoverlapping, or uncorrelated. On the other hand, ions with similar mass and size, for example ions of proteins and metal particles, can show totally different "the field dependence of the mobility" because of their internal structures and bond strength. The field dependence of the mobility is quite independent of and orthogonal to mass and other properties.

Those independence and orthogonality, conversely, are employed to separate or to distinguish ions with similar mass and size, which is usually very difficult for MS. For this property FAIMS is mainly utilized as a filter for MS to select interest ions from background of solvents in ESI and of matrices in MALDI. There are many those kinds of pre-stage filter for MS. However FAIMS shows much higher performance especially for ions with similar mass and chemical properties. Those ions are difficult to be identified only by MS even with other chemical filtering processes such as liquid chromatography. FAIMS can select those ions with the difference in the field dependence of mobility. On the contrary, the low field IMS distinguish with the cross section which has close relationship with the size and the mass, which suggests that ions with similar size and mass are selected in the almost same condition resulting in its low performance as a filter.

With the improvement of the resolution of FAIMS, the method now begins to be utilized for more advanced purposes such as manipulation of molecules and investigation of ion–molecule interaction [2, 9, 15]. For example, amino acid molecules with hydrogen/deuterium, $^{12}C/^{13}C$, and $^{14}N/^{15}N$ exchanges show different FAIMS profiles [35]. Those isotopomer ions with the same mass constructed by the combination of these exchanges also show the different properties in FAIMS, which have not been observed by the low field IMS. It is difficult to explain the origin of the effect, but their differences in the vibrational and the rotational states and those in the long range interaction may cause the results [35].

6.4 Applications

IMS has long history especially in aerosol science and security area as described in Sect. 6.1 and has wide application fields [2]. Here structural studies on nanomaterials and detection of molecular interaction between chiral species are shown, since the main topic of this book is MS which has been a major tool for nanomaterials and biomolecules. Especially in biomolecules the interaction like chiral selectivity is one of the key issues [36]. Both of them show structural varieties and their properties are strongly dependent on the structures to which IMS clearly provides important information. Many research articles on bio-related molecules are published [36]; so chiral molecular detection is described here together with nanomaterials.

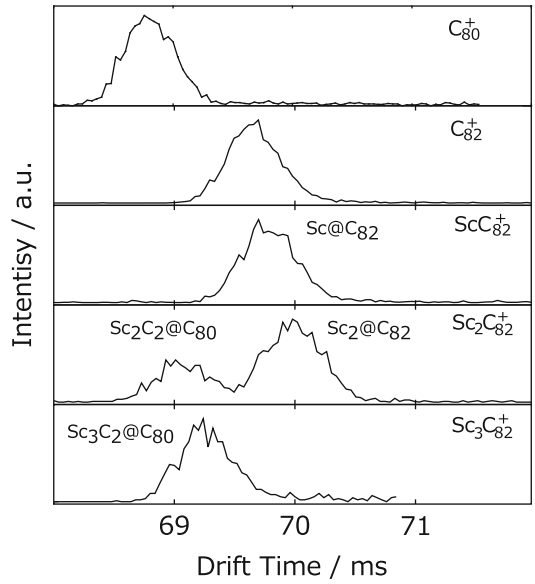

Fig. 6.8 High-resolution ion mobility profiles of C_{80}^+, C_{82}^+ and $Sc_nC_{82}^+$ ($n = 1$–3) produced from laser desorption/ionization of solvent extractable fullerenes. $Sc_2C_{82}^+$ shows two distinct peaks (details see text)

6.4.1 Metallofullerene

Fullerene is one of the most significant nanomaterials as the first atomically identified and purified ones. Fullerene consists of around 100 carbon atoms with spherical shell structures and shows various distinct and useful properties which are determined by the structures. One of them is hollow inside space which can hold other molecules and materials resulting in modified structures and properties [37]. By changing the number of atoms inside and changing outside fullerene structures, those properties are controlled so that the structural studies on whole species are crucial. For these materials conventional structural analyses have been performed by NMR and X-ray diffraction together with isolation. Fullerenes like other nanomaterials are produced as mixtures through vapor condensation processes. Those mixtures are difficult to purify, which require several months to prepare mg order isolated samples with HPLC separation. The HPLC separation requires not only huge efforts but also dissolution in organic solvents so that some of the fullerenes cannot be studied by their low solubility. As a result, atomically resolved nanomaterials known up to now are not so rich: a part of fullerenes, noble metal clusters, and carbon nanotubes. To expand structural studies on other nanomaterials by improving efficiency and by applying comprehensive structural analyses, IMS/MS is one of the best methods in terms of direct treatment and high throughput on mixture samples without pre-purification.

Figure 6.8 shows drift time profiles for positive ions of empty fullerenes and metallofullerenes obtained from solvent extractable C_{80}, C_{82}, and Sc_nC_{82} ($n = 1$–3) using the IMS/MS apparatus shown in Fig. 6.5. C_{80}^+ and C_{82}^+ have a single peak and the drift time of C_{80}^+ is clearly shorter than that of C_{82}^+. Simple analyses of the drift time in Eq. (6.18) show that their spherical structures exactly correspond to those obtained by X-ray [37, 38] and computational calculation [39]. Those results show that fullerene structures are not disturbed by the laser desorption/ionization, and the structural resolution of the apparatus is good enough to identify the fullerene size but is not sufficient to resolve structural isomers [39]. The ion of $Sc@C_{82}^+$ also shows a single peak which exactly corresponds

to that of C_{82}^+ and well-annealed C_{82}^+ clusters [22, 40]. These results are consistent with the endohedral structures determined by X-ray diffraction [38]. On the other hand, the di-metallofullerene $Sc_2C_{82}^+$ shows two distinct peaks. The main peak with larger drift time and larger cross section corresponds to the peaks of C_{82}^+ and $Sc@C_{82}^+$. The other peak has a substantially smaller drift time which is very similar to that of C_{80}^+ revealing that some of $Sc_2C_{82}^+$ has C_{80} cage. The tri-metallofullerene $Sc_3@C_{82}^+$ shows only one peak close to C_{80}^+. The high-resolution ion mobility measurements enable us to detect these two structures for the first time.

One of the significant merits of IMS observation is investigation on whole species. In terms of Sc mono-metallofullerenes in the size region less than C_{100}, their cross section is almost same as those of the corresponding empty fullerenes, which indicates that Sc metallofullerenes have endohedral structures of $Sc@C_n$. In contrast, most of $Sc_2C_n^+$ ($n \leq 86$) have two cage sizes: one corresponds to that of C_n^+ and the other corresponds to that of C_{n-2}^+. These results strongly suggest that $Sc_2C_n^+$ ions have a "carbide" structure like $(Sc_2C_2)@C_{n-2}^+$ as well as $Sc_2@C_n^+$ of the simple endohedral structure. Larger Sc di-metallofullerenes $Sc_2@C_n^+$ ($n \geq 88$) and Sc tri-metallofullerenes $Sc_3@C_n^+$ only have the smaller cage. These Sc tri-metallofullerenes may also possess carbide $(Sc_3C_2)@C_{n-2}^+$ structures. The drift time of the metallofullerenes is slightly larger than that of corresponding empty fullerenes (cf. Fig. 6.8). These differences are probably associated with the electronic properties of the metallofullerenes. Electrons are transferred from the metal atoms to the cage, which resulted in, for example, $Sc^{2+}@C_{82}^{2-}$ [38]. Since the ion mobility is mainly dominated by close interaction between the fullerene cage and He [41], $(Sc^{2+}@C_{82}^{2-})^+$ and C_{82}^+ are expected to have slightly different mobilities [42].

Since this IMS/MS measurement requires the laser desorption/ionization, the carbide structures may be generated through the processes. The laser power dependence of $Sc_2@C_{82}^+$ shows that the carbide structures are preferred in the large power condition suggesting the laser-induced reactions from the normal to the carbide. Although these new carbide structures are observed in gas phase upon desorption/ionization, we have produced and identified $(Sc_2C_2)@C_{84}$ in macroscopic quantities [43]. The other group recently has identified this carbide structures of $(Sc_3C_2)@C_{80}$ for Sc tri-metallofullerenes [44]. The results presented here show that the carbide encapsulated structure are universal in the wide size range. The results also clarified that novel structures can be identified by series of IMS/MS measurements utilizing its high sensitivity and high throughput, which is available for mixtures and wide range of materials.

6.4.2 Chiral Detection

The chiral detection has been a key issue for MS but is difficult to be realized [45]. Usually chiral molecules are identified by optical activity or chiral columns. Those methods are the so-called bulk methods requiring large amount of isolated samples. High sensitive method like MS has been waited for long term. Even though the interaction difference between chiral molecules can affect the dissociation pattern [45], the difference is usually too small to be detected in dissociation processes. However this small difference is apparently observed by IMS with a sum effect through many collisions as described in Sect. 6.1.2 [46, 47, 48].

Simple chiral molecules are investigated by a differential pumping type IMS/MS where chiral (*S*)-(+)-2-butanol and (*R*)-(−)-2-butanol are doped in the buffer gas of the IMS cell with the order of ppm [46]. When the ion and the dopant have the same chirality, a longer drift time or stronger interaction is observed indicating that the chiral interaction is intense enough to be detected with the cross section difference to the order of 10^2–10^3 between the chiral pairs. The origin of this chiral

dependence and the generality should be investigated, but the results show the potential and the sensitivity of IMS as a tool for molecular investigation. FAIMS also reveals this chiral dependence [48].

Other chiral dependence is found in spontaneous crystallization of proline clusters ($[\mathrm{Pro}_x + n\mathrm{H}]^{n+}$, $x = 40$–100, $n = 4, 5$) [47]. Pure D-proline or L-proline forms rod-like clusters, whereas racemic mixtures of proline form globular clusters. The rod-like clusters from pure D-proline and L-proline have exactly the same mobility suggesting symmetrical structures of those clusters. If we consider those clusters a type of bulk crystals, the chiral dependence of the cluster structures may be attributed to spontaneous crystallization and spontaneous optical resolution.

Those two researches show that IMS has very high sensitivity to detect fine molecular interaction which should come from many collisions and summed effects in the cell described in Sect. 6.1.2

6.5 Summary

IMS has similarity with MS as a method detecting charged particles. They are now combined as the hybrid measurement system of IMS/MS, which is now a key tool to investigate bio and medical sciences, nano and material technologies. The structural observation and utilization of low energy processes provide a new aspect to MS. The wide range applications and new sciences are realized by this method. However understanding and analysis of the observed information are not simple since the measurement is performed through the many collisions between ions and gas molecules where the interaction between them are statistically averaged. To understand the obtained results and elucidate more information, the study and analysis on the basic processes in IMS are still necessary. Computational investigation would play significant roles for further analyses. Technically relatively low resolution and low sensitivity compared to MS are ongoing problems. RF devices, vacuum technology, and fluid dynamics have been utilized to overcome those difficulties. Even with these problems and difficulties, IMS/MS has huge potential in wide range fields. This method provides not only structural information but also detection of weak molecular interaction by utilization of wide range of E/N. They have been developed to realize sophisticated chirality detection and manipulation of molecules. The measurement system has been rapidly developed by various groups to be commercialized. I hope that this measurement be more and more common globally and be applied to much wider area, which would lead us to the next stage of science and technology.

References

1. Mason EA, McDaniel EW (1988) Transport properties of ions in gases. Wiley, New York
2. Eiceman GA, Karpas Z (2005) Ion mobility spectroscopy. CRC, Boca Raton
3. Kroto HW, Heath JR, O'Brien SC, Curl RF, Smalley RE (1985) Nature 318:162
4. Krätschmer W, Lamb LD, Fostiropoulos K, Huffman DR (1990) Nature 347:354–358
5. Taylor R, Hare JP, Abdul-Sada AK, Kroto HW (1990) J Chem Soc Chem Commun 20:1423–1425
6. Hawins JM, Meyer A, Lewis TA, Loren S, Hollander FJ (1991) Science 252:312–313
7. von Helden G, Hsu MT, Kemper PR, Bowers MT (1991) J Chem Phys 95:3835–3837
8. von Helden G, Hsu MT, Gotts N, Bowers MT (1993) J Phys Chem 97:8182–8192
9. Sugai T (2010) J Mass Spectrom Soc Jpn 58:47–73
10. Revercomb HE, Mason EA (1975) Anal Chem 47:970
11. Berry RS, Rice SA, Ross J (2000) Physical chemistry. Oxford University Press, New York
12. Sugai T, Inakuma M, Hudgins R, Dugourd P, Fye JL, Jarrold MF, Shinohara H (2001) J Am Chem Soc 123:6427–6428
13. Tabrizchi M, Rouholahnejad F (2006) Talanta 69:87–90
14. Nazarov EG, Coy SL, Krylov EV, Miller RA, Eiceman GA (2006) Anal Chem 78:7697–7706

15. Shvartsburg AA (2009) Differential ion mobility spectrometry: nonlinear ion transport and fundamentals of FAIMS. CRC, New York
16. Tanuma H, Sakamoto M, Fujimatsu H, Kobayashi N (2000) Rev Sci Instrum 71:2019–2024
17. Hidaka H, Jinno S, Tanuma H, Kobayashi N (2003) J Phys B At Mol Opt Phys 36:1515–1524
18. Levine RD, Bernstein RB (1987) Molecular reaction dynamics and chemical reactivity. Oxford University Press, New York
19. Merenbloom SI, Bohrer BC, Koeniger SL, Clemmer DE (2007) Anal Chem 79:515–522
20. Merenbloom SI, Glaskin RS, Henson ZB, Clemmer DE (2009) Anal Chem 81:1482–1487
21. Kuk Y, Jarrold MF, Silverman PJ, Bower JE, Brown WL (1989) Phys Rev B 39:11168
22. Shelimov KB, Jarrold MF (1996) J Am Chem Soc 118:1139–1147
23. McDaniel EW, Martin DW, Barnes WS (1962) Rev Sci Instrum 33:2–7
24. Dugourd P, Hudgins RR, Clemmer DE, Jarrold MF (1997) Rev Sci Instrum 68:1122–1129
25. Ruotolo BT, McLean JA, Gillig KJ, Russell DH (2004) J Mass Spectrom 39:361–367
26. Tang K, Shvartsburg AA, Lee H-N, Prior DC, Michael FL, Buschbach A, Tolmachev AV, Anderson GA, Smith RD (2005) Anal Chem 77:3330–3339
27. Merenbloom SI, Koeniger SL, Valentine SJ, Plasencia MD, Clemmer DE (2006) Anal Chem 78:2802–2809
28. Giles K, Pringle SD, Worthington KR, Little D, Wildgoose JL, Bateman RH (2004) Rapid Commun Mass Spectrom 18:2401–2414
29. Takada Y, Nagano H, Suzuki Y, Sugiyama M, Nakajima E, Hashimoto Y, Sakairi M (2011) Rapid Commun Mass Spectrom 2011:2448–2452
30. Williams JP, Scrivens JH (2008) Rapid Commun Mass Spectrom 22:187–196
31. Shvartsburg AA, Smith RD (2008) Anal Chem 80:9689–9699
32. Bush MF, Hall Z, Giles K, Hoyes J, Robinson CV, Ruotolo BT (2010) Anal Chem 82:9557–9565
33. Buryakov IA, Krylov EV, Nazarov EG, Rasulev UK (1993) Z Phys 128:143–148
34. Shvartsburg AA, Smith RD, Wilks A, Koehl A, Ruiz-Alonso D, Boyle B (2009) Anal Chem 81:6489–6495
35. Shvartsburg AA, Clemmer DE, Smith RD (2010) Anal Chem 82:8047–8051
36. Wyttenbach T, Bowers MT (2007) Annu Rev Phys Chem 58:511–533
37. Shinohara H (2000) Rep Prog Phys 63:843–892
38. Nishibori E, Takata M, Sakata M, Inakuma M, Shinohara H (1998) Chem Phys Lett 298:79–84
39. Kobayashi K, Nagase S (1998) Chem Phys Lett 282:325–329
40. Shvartsburg AA, Hudgins RR, Dugourd P, Gutierrez R, Frauenheim T, Jarrold MF (2000) Phys Rev Lett 84:2421–2424
41. Clemmer DE, Jarrold MF (1997) Int J Mass Spectrom 32:577–592
42. Lermé J, Dugourd P, Hudgins RR, Jarrold MF (1999) Chem Phys Lett 304:19–22
43. Wang CR, Kai T, Tomiyama T, Yoshida T, Kobayashi Y, Nishibori E, Takata M, Sakata M, Shinohara H (2001) Angew Chem Int Ed 40:397–399
44. Iiduka Y, Wakahara T, Nakahodo T, Tsuchiya T, Sakuraba A, Maeda Y, Akasaka T, Yoza K, Horn E, Kato T, Liu MTH, Mizorogi N, Kobayashi K, Nagase S (2005) J Am Chem Soc 127:12500–12501
45. Tao WA, Zhang D, Wang F, Thomas PD, Cooks RG (1999) Anal Chem 71:4427–4429
46. Dwivedi P, Wu C, Matz LM, Clowers BH, Siems WF, Herbert J, Hill H (2006) Anal Chem 78:8200–8206
47. Myung S, Fioroni M, Julian RR, Koeniger SL, Baik M-H, Clemmer DE (2006) J Am Chem Soc 128:10833–10839
48. Mie A, Jörntén-Karlsson M, Axelsson B-O, Ray A, Reimann CT (2007) Anal Chem 79:2850–2858